ISSN 0915-633X

NATIONAL INSTITUTE FOR FUSION SCIENCE

Non-local Simulation of the Formation of Neoclassical Ambipolar Electric Field in Non-axisymmetric Configurations

S. Satake, M. Okamoto, N. Nakajima, H. Sugama and M. Yokoyama

(Received - Oct. 25. 2005)

NIFS-827 Nov. 2005

RESEARCH REPORT
NIFS Series

TOKI, JAPAN

Non-local Simulation of the Formation of Neoclassical Ambipolar Electric Field in Non-axisymmetric Configurations

SATAKE Shinsuke, OKAMOTO Masao, NAKAJIMA Noriyoshi, SUGAMA Hideo, and YOKOYAMA Masayuki

National Institute for Fusion Science, Toki, Japan

Abstract

Neoclassical transport simulation code (FORTEC-3D) applicable to non-axisymmetric configurations is developed. Adoption of a new hybrid simulation model, in which ion transport is solved by using the δf Monte-Carlo method including the finite-orbit-width effects while electron transport is solved by a reduced ripple-averaged kinetic equation, makes it possible to simulate the dynamism of non-local transport phenomena with self-consistently developing radial electric field within a allowable computation time. Time evolution of radial electric field in LHD plasma is simulated in the full volume of confinement region, and the finite-orbit-width effect of neoclassical transport is found to make the negative ambipolar electric field more larger than the prediction by a local transport theory.

keywords : neoclassical transport, ambipolar electric field, finite-orbit-width effect

1 Introduction

Neoclassical transport theory has been successfully established under the assumption of the local transport model(small-orbit-width limit) and in a quasi-steady state. However, these assumptions cannot be used to investigate those issues which have been attracting much interests recently, such as the finite-orbit-width (FOW) effects when the typical orbit width in the radial direction is comparable to the background gradient scale, the geodesic acoustic mode (GAM) of electric field and its Landau damping mechanism[1], and the evolution of ambipolar radial electric field E_r. Though the net radial transport level observed in experiments is usually dominated by anomalous transport, self-induced electric field profile can be explained by the neoclassical transport theory. We have shown[2] by a Monte-Carlo simulation using the δf method[3, 4] that a steep E_r profile can be formed if there exists a steep density gradient in tokamak cases. Such a sheared E_r profile is considered to reduce both neoclassical transport level by the orbit-squeezing effect[5] and microscopic turbulence by $E \times B$ shearing effect. In non-axisymmetric cases, steep shear in E_r profile can also be formed if the ambipolar condition has multiple solutions[6]. Since the neoclassical fluxes in helical plasma strongly depend on E_r, the determination of radial electric field in the existence of multiple ambipolar roots is a key issue to evaluate transport level in helical plasma.

The transition and bifurcation phenomena of E_r in helical systems have usually been studied by using analytic model for neoclassical transport[7, 8], for example in [6, 9]. These previous studies have put a focus on relatively slow time scale phenomena, that is, the transport time scale in which background profile of density and temperature change. We are interested in a more short time scale phenomena comparable to transit time $\tau_{tr} \sim qR/v_{th}$ to ion collision time τ_i where the background n and T profiles can be considered unchanged and in the non-local effects in neoclassical transport. However, the analytic model of neoclassical transport lacks these physical mechanisms as follows: 1) GAM oscillation and polarization drift motion associated with rapid time evolution of radial electric field, 2) non-local drift motion of transit particle orbits in non-axisymmetric configuration and its contribution to neoclassical transport, 3) direct orbit loss at the plasma boundary, and 4) rigorous treatment for Coulomb collision. To simulate the dynamic transport process and formation of ambipolar electric field including non-local effects in non-axisymmetric configurations, we have been developing the δf code FORTEC-3D to be applicable to general 3-dimensional configurations. The formulation is explained in Sec. 2. In FORTEC-3D, ion neoclassical transport is solved by the δf method while electron one is obtained

from a ripple-averaged kinetic equation solver GSRAKE[10, 11], and the time evolution of E_r is solved self-consistently in the simulation. The adoption of this hybrid simulation model enables us to simulate neoclassical transport including the FOW effect of ions within a allowable computation time. For a demonstration of the new simulation model, we show in this paper the global simulation results of time evolution of radial electric field in LHD plasmas in Sec. 3. The formation of ambipolar E_r profile in the presence of multiple roots for ambipolar condition is successfully simulated, and it is found that the FOW effect changes the ambipolar electric field profile from that obtained by a conventional local transport analysis.

2 Simulation model

In the δf method, time development of the perturbation of plasma distribution function from local Maxwellian $\delta f = f - f_M$ is solved according to the drift-kinetic equation

$$\begin{aligned} \frac{D\delta f}{Dt} &\equiv \frac{\partial \delta f}{\partial t} + \left(\mathbf{v}_\parallel + \mathbf{v}_d\right) \cdot \nabla \delta f - C_{tp}(\delta f) \\ &= -\mathbf{v}_d \cdot \nabla f_M + \mathcal{P} f_M, \end{aligned} \tag{1}$$

where C_{tp} and $\mathcal{P}$ are test-particle and field-particle parts of linearized collision operator, $\mathbf{v}_\parallel = \mathbf{v} \cdot \mathbf{B}/B$, and $\mathbf{v}_d$ is the drift velocity of guiding center motion across the magnetic field line. The magnetic field is given in the Boozer coordinate system (ψ, θ, ζ)[12] as $\mathbf{B} = \nabla\psi \times \nabla\theta + \iota \nabla\zeta \times \nabla\psi$, where ψ is the toroidal flux, θ and ζ are poloidal and toroidal angle, and ι is the rotational transform divided by 2π, respectively. In our simulation, the magnetic field configuration is constructed from VMEC code[13] which solves MHD equilibrium state for a given pressure and plasma current profiles. The guiding center equations of motion in the Boozer coordinates is also described in [12]. The guiding center motion of simulation markers, of which distribution function is expressed as g here, is traced in 5-dimensional phase space $(\psi, \theta, \zeta, v_\parallel, v_\perp)$. The test-particle collision operator C_{tp} is implemented numerically by random kicks of marker velocity in the $(v_\parallel, v_\perp)$ space. Then $\mathcal{P} f_M$ is defined so that the three constants in exact Fokker-Planck collision operator, i. e., total particle number, moments, and energy, should really be conserved. The detail of collision operator used here is described in [3]. To solve eq. (1), two weights w and p are introduced which satisfy the relations $wg = \delta f$ and $pg = f_M$. Since the time evolution of marker distribution can be described by $Dg/Dt = 0$, where D/Dt means the total derivative along

marker motion including stochastic motion by the effect of C_{tp}, these weights evolve according to

$$\frac{dw}{dt} = \frac{p}{f_M}\left[-\mathbf{v}_d\cdot\nabla + \mathcal{P}\right] f_M, \tag{2a}$$

$$\frac{dp}{dt} = \frac{p}{f_M}\mathbf{v}_d\cdot\nabla f_M. \tag{2b}$$

Note that the FOW effect is included from $\mathbf{v}_d\cdot\nabla\delta f$ term in eq. (1), which is omitted in standard neoclassical theory.

Neoclassical particle and energy fluxes are evaluated by

$$\Gamma = \left\langle \int d^3v \dot{\psi}\delta f \right\rangle, \tag{3a}$$

$$q = \left\langle \int d^3v \frac{1}{2}mv^2\dot{\psi}\delta f \right\rangle, \tag{3b}$$

where $\langle\cdots\rangle$ means the flux-surface average. The time evolution of radial electric field $\mathbf{E} = -d\Phi/d\psi\nabla\psi = E_\psi\nabla\psi$ can be described as follows

$$\epsilon_0\left[\left\langle|\nabla\psi|^2\right\rangle + \left\langle\frac{c^2}{v_A^2}|\nabla\psi|^2\right\rangle\right]\frac{\partial E_\psi}{\partial t} = -e\left[z_i\Gamma_i - \Gamma_e\right], \tag{4}$$

where subscripts i and e describe particle species, and v_A is the Alfvén velocity. The term containing v_A appears because of the classical polarization drift proportional to $\partial\mathbf{E}/\partial t$. The neoclassical polarization drift, which can be explained by considering the drift of bounce-averaged position $\oint dt\dot{\psi}/\tau_b$ when E_ψ is time-dependent, is essentially included in the evaluation of eq. (3) because we trace the marker orbit directly in the time-dependent field without any averaging operation in solving the equations of motion. Similarly, the orbit squeezing effect is also included in eq. (3) since marker orbit is traced exactly including the radial excursion in a sheared E_ψ field.

In our previous study for tokamak plasmas, electron particle flux Γ_e has been neglected because of the smallness of it. In non-axisymmetric cases, however, Γ_e becomes comparable to Γ_i and is needed in order to simulate the time evolution of ambipolar electric field in which $\Gamma_e(\psi, E_\psi) = z_i\Gamma_i(\psi, E_\psi)$ is satisfied. The hybrid simulation model for evaluating Γ_e and Γ_i introduced in Sec. 1 is adopted since the FOW effect is expected to be important mainly on ions which have wider radial orbit width than electrons. The details of GSRAKE code used to evaluate Γ_e are found in the references[10, 11]. We would only explain it here briefly. GSRAKE solves ripple-averaged (or so-called bounce-averaged) kinetic equation in helical systems. One advantage of GSRAKE to other analytic models is that it treats both ripple-trapped particles and non-localized (passing) particles on an equal foot in the formulation. It can be applicable to the whole long-mean-free-path regime ($\nu_{eff}/\tau_b << 1$) and wide range of E_ψ. Therefore, it is suitable to make the table

of $\Gamma_e(\psi, E_\psi)$ in the entire simulation domain (ψ, E_ψ) where the collisionality and E_ψ may change largely. The Γ_e-table is then referred on each step in FORTEC-3D to evaluate eq. (4). The reliability of the result of GSRAKE in LHD configuration has been benchmarked in the above references.

Because a magnetic coordinate system is used, we have no information beyond the last closed flux surface (LCFS). The magnetic field spectrum is extrapolate to the outer region, and markers which spend some time steps out of the LCFS are killed and recycled inside the LCFS. The procedure corresponds to a orbit-loss mechanism at the boundary. Recycled marker weights should be determined so as not to bring any physical value such as particle density, momentum, and energy into the rebirth point. For the weight w, the easiest way is to set the new weight $w = 0$ for recycled markers. However, it causes a numerical noise because these recycled markers enhance the spreading of weight field variance. In fact, the weight spreading is essentially inevitable in the δf method[4] because two markers which have moved on different paths in the phase space come up to the same point at the same time with bringing different weights. We have expanded the weight-averaging technique described in Ref.[4] for the determination of new marker's weights as follows. (Though we only show the procedure for weight w here, it can also be applied in determining p.)

At first, consider an averaged weight field $W_{ij}(\mathbf{v})$ in a small bin (i, j) in the velocity space $(v_\parallel, v_\perp)$. We assume that W_{ij} is given in the following form

$$W_{ij}(\mathbf{v}) = W_{ij}^{(0)} + W_{ij}^{(1)} v_\parallel + W_{ij}^{(2)} v^2. \tag{5}$$

Next, the weight for existing markers w_k and newly recycled ones w_l in the (i, j) bin are renewed toward $W_{ij}(\mathbf{v})$ with a damping rate γ $(0 < \gamma < 1)$,

$$w_k^1 = \gamma W_{ij}(\mathbf{v}_k) + (1-\gamma) w_k^0, \tag{6a}$$

$$w_l^1 = W_{ij}(\mathbf{v}_l), \tag{6b}$$

where overscripts 0 and 1 denote the old and new value. To make the sums of constants-of-motion in a bin unchanged on recycling, the following relations must be satisfied.

$$\sum_k w_k^0 = \sum_k w_k^1 + \sum_l w_l^1, \tag{7a}$$

$$\sum_k w_k^0 v_{\parallel k} = \sum_k w_k^1 v_{\parallel k} + \sum_l w_l^1 v_{\parallel l}, \tag{7b}$$

$$\sum_k w_k^0 v_k^2 = \sum_k w_k^1 v_k^2 + \sum_l w_l^1 v_l^2. \tag{7c}$$

Combining eqs. (5)-(7) one obtains the following relation, which is inverted to determine $W_{ij}^{(0,1,2)}$,

$$\gamma \begin{pmatrix} \sum_k w_k^0 \\ \sum_k w_k^0 v_{\parallel k} \\ \sum_k w_k^0 v_k^2 \end{pmatrix} = \begin{pmatrix} \gamma k_{ij} + l_{ij} & \sum_{k,l} \gamma v_{\parallel k} + v_{\parallel l} & \sum_{k,l} \gamma v_k^2 + v_l^2 \\ & \sum_{k,l} \gamma {v_{\parallel}}_k^2 + {v_{\parallel}}_l^2 & \sum_{k,l} \gamma v_{\parallel k} v_k^2 + v_{\parallel l} v_l^2 \\ & & \sum_{k,l} \gamma v_k^4 + v_l^4 \end{pmatrix} \cdot \begin{pmatrix} W_{ij}^{(0)} \\ W_{ij}^{(1)} \\ W_{ij}^{(2)} \end{pmatrix}, \tag{8}$$

where the matrix is symmetric, and $k_{ij},\ l_{ij}$ are numbers of existing and recycling markers in a bin, respectively. We have checked the recycling procedure worked well without increasing the weight variance at the rebirth region for 6000 computation time step which corresponds to $t = 3.0\tau_i$. By introducing the recycling technique, it is possible to trace the time evolution of radial electric field up to a few collision times which is required to simulate the transport phenomena until the distribution function δf comes to a quasi-steady state.

3 Transport simulation in LHD plasma

We have conducted transport simulation using FORTEC-3D in several configurations. The magnetic field configuration is constructed modeled on a LHD plasma[14] in which the magnetic axis and magnetic field strength on it are $R_{ax} = 3.7$m and $B_0 = 1.65$T, respectively. The density and temperature profiles for ions and electrons are given by the following expression

$$\begin{Bmatrix} n_{i,e}(\rho) \\ T_{i,e}(\rho) \end{Bmatrix} = \begin{Bmatrix} n_{0i,e} \\ T_{0i,e} \end{Bmatrix} \left[\alpha_1 + (1-\alpha_1)\exp(-\alpha_2 \rho^{\alpha_3})\right], \tag{9}$$

where $\rho = \sqrt{\psi/\psi_{edge}}$ is the normalized minor radius, $(\alpha_1, \alpha_2, \alpha_3) = (-0.01, 3.0, 3.5)$ for density and $= (0.05, 4.5, 2.0)$ for temperature, respectively. In the first case, we set $T_{0i} = T_{0e} = 1.0keV$ and $n_{0i} = n_{0e} = 2.0 \times 10^{18} m^{-3}$. The plasma collisionality is considered to be in the $1/\nu$ regime[15] almost in the entire plasma region. We have used $60 \times 20 \times 10$ meshes in the ψ, θ, and ζ-directions respectively, and 20×10 meshes in the velocity space $(v_\parallel, v_\perp)$. The simulation domain is restricted in one-helical pitch ($0 < \zeta < \pi/5$) and a cyclic boundary condition is set in the ζ-direction. 64 millions of markers have been used in the simulation. Such a large number of markers are required to suppress the statistical noise in the long-time simulation up to few collision times. Though the simulation becomes heavy in the 3-dimensional cases, it takes only 10 hours to run up to $1.0\tau_i$ on the supercomputer system in NIFS owing to the high parallelization and vectorization efficiency of the code written in HPF (High Performance Fortran).

Figure 1 shows the radial electric field profile formed at a quasi-steady state at $t = 0.5\tau_i$, where τ_i is evaluated at $\rho = 0.5$. In this figure, the guess of the ambipolar E_r profile is predicted by solving Γ_i as well as Γ_e from GSRAKE to seek the root that satisfies $\Gamma_e(E_r) = \Gamma_i(E_r)$ on each radial position. We show here two guesses from GSRAKE by turning on/off the contribution of $\partial B/\partial\rho$ term in the ripple-averaged kinetic equation. This term is related to the poloidal component of ∇B drift motion. Γ_i obtained from GSRAKE shows somewhat a oscillatory behavior on the change of E_r if the $\partial B/\partial\rho$ term is included, while Γ_e is not so much affected by this term. Therefore, we show in Fig. 1 some candidates of the solution for ambipolar E_r obtained from GSRAKE calculated with $\partial B/\partial\rho$ term. Neglecting this term make the estimated ambipolar-$|E_r|$ value a little smaller as can be seen in Fig. 1. In both cases, it is predicted that there is only a negative root (ion root) in the entire region, and the result of FORTEC-3D is also settled in a negative E_r profile. In the outer-half of the plasma $\rho > 0.5$, the ambipolar E_r value from FORTEC-3D and from GSRAKE differs as much as 50%. The reason of this difference seems to be because the ripple-averaged kinetic equation neglects these physics which are contained in the δf formulation, such as the FOW effect, rigorous treatments of collision term, and exact drift motion without averaging over a bounce time. Among them, we expect that the major effect which makes the difference in E_r is the FOW effect, especially for a low-collisionality plasma. Further inspection is shown later. On the contrary, as shown in figure 2, ambipolar flux obtained from FORTEC-3D shows a good agreement with the predictions from GSRAKE both in the case with- and without-$\partial B/\partial\rho$ term to make the $\Gamma_{i,e}$-tables. Since Γ_i generally has a steep peak on the negative side close to $E_r = 0$ as illustrated in figure 3, it is expected that a small difference of Γ_i between FORTEC-3D and GSRAKE by non-local effect would change the ambipolar condition if the root is close to the peak position. In Fig. 3, one can also see that ambipolar flux changes only slightly on the change of the ambipolar E_r because Γ_e is insensitive to the change of E_r compared with Γ_i.

As concerns the non-local effects on ion transport considered in FORTEC-3D , it can be classified them into two. One is the finiteness of radial drift widths of helically and toroidally trapped orbits. In tokamaks, trapped particles sometimes have a orbit width as large as several tens % of the minor radius, and we have shown that neoclassical heat flux and ambipolar condition in tokamaks are affected by the FOW effect of the large potato orbits appearing in the core region of tokamaks[16, 17]. In helical LHD configuration, however, the orbit width of helically trapped particles is small and its FOW effect is expected to be weak. A more strong effect on neoclassical transport in LHD will arise from the FOW effect of transit orbits, which show a transition between

helically and toroidally trapped (or passing) orbits. If the collisionality is small, some ion particles can drift a long distance in the radial direction by transitions. The other is the direct orbit loss at the plasma boundary. In FORTEC-3D, this effect is included by killing the simulation markers which escape from the LCFS. Since we neglect the precise loss mechanisms of bulk ions by collisions between neutrals or impurities and the real orbit in a stochastic magnetic field at the peripheral region are not included, our simulation is regarded as a simple model of orbit loss by a virtual limiter placed close to the LCFS.

In order to investigate these non-local effects on the formation of ambipolar electric field, we carried out two simulations : (a) by changing the strength of magnetic field 4 times larger (though it is not achievable in real LHD experiment) than in the case shown in Fig. 1, and (b) by changing magnetic axis position to $R_{ax} = 3.6$m. In both simulation, n and T profiles are the same as in the previous case. Before explaining the simulation result, we mention here the collisionality in these simulations. The collisional regime of helical plasma is usually classified by the normalized factor $\nu_h^* \equiv qR_0\nu_i/v_{th}\epsilon_h^{3/2}$ for a single-helicity case, where $\nu_i = \tau_i^{-1}$ and $\epsilon_h = B_{l,m}/B_0$ describes the relative magnitude of the Fourier component of the helical field. Though there is a proper definition for ϵ_h for a multi-helicity case[15], we use an approximation that $\epsilon_h \simeq B_{2,10}/B_0$ as $B_{2,10}$ is the major helical component for a LHD configuration. The other two parameters used here to distinguish the plasma collisionality are $\nu_{eff} \equiv \nu_i/\epsilon_h$ and $\omega_E = |E_r|/rB_0$, which represent the effective collisionality for ripple-trapped particles and the $E \times B$ rotational frequency, respectively. In the simulation shown here, for example at $\rho = 0.7$ in the $R_{ax} = 3.7$ case, these parameters are $\epsilon_h = 0.12,\ \nu_h^* = 0.36,\ \nu_{eff} = 3.9 \times 10^3$, and $\omega_E = 4.0 \times 10^3$. These parameters is almost the same in the $R_{ax} = 3.6$ case shown below. Since $\nu_h^* \ll 1$, the plasma is well in the $1/\nu$ regime. Moreover, $\omega_E \simeq \nu_{eff}$ means that the collisional regime is around the transition layer from the $1/\nu$ regime to $\nu^{1/2}$ regime, where the collisionless transition between trapped and untrapped orbits as well as the collisional diffusion of ripple-trapped particles contribute the radial transport. In this collisionality, the radial transport level strongly depends on E_r (diffusion coefficient $D \sim 1/\nu E_r$ in the $1/\nu$ regime and $\sim \nu^{1/2}/E_r^{3/2}$ in the $\nu^{1/2}$ regime[15]), and the finiteness of the transition particle orbit is expected to be effective on the particle transport.

Now let us see the simulation results in Fig. 4 and 5. In the strong B-field case, discrepancy in the ambipolar E_r between GSRAKE and FORTEC-3D is small in the edge region $\rho > 0.8$, while a clear difference remains in the core region $0.2 < \rho < 0.8$. If the magnetic axis is shifted to $R_{ax} = 3.6$m, one can see that the discrepancy in the ambipolar E_r becomes smaller than that in the case $R_{ax} = 3.7$m. It is known that in LHD plasma, neoclassical transport level is suppressed

by shifting the magnetic axis inward[18]. In the view of single particle orbit, this improvement of plasma confinement is because radial excursion of transit orbit in a inwardly shifted configuration is shrunk according as the Fourier components of the magnetic field spectrum change toward a "σ-optimized" field[19]. Therefore, non-local effect brought by transit particles, which is correctly evaluated in the δf simulation, is expected to be less effective on the total neoclassical transport in the case $R_{ax} = 3.6$m, and then the ambipolar E_r obtained from FORTEC-3D is close to the result from GSRAKE, which is a small-orbit-width transport model. On the other hand, improvement in confinement of transit orbit is not expected by changing only the absolute strength of the magnetic field. Note here that, since plasma pressure is very low ($\beta \sim 0.01\%$) in the simulations we show here, relative magnitude of each Fourier component of magnetic field is almost fixed on the change of absolute strength of it. From the result shown in Fig.4, it is considered that the orbit loss transport at the edge region is suppressed because strong magnetic field shrinks the orbit width of toroidally trapped particles, and the difference of ambipolar E_r between GSRAKE and FORTEC-3D becomes smaller in the strong B-field case. The discrepancy of the ambipolar E_r between $0.2 < \rho < 0.8$ seems larger for the strong magnetic field case in Fig. 4. Note here that the $E \times B$ drift, which reduce the radial particle drift and transport in the collisionless regime, is proportional to E_r/B. From the result of FORTEC-3D simulation in Fig.4, the fraction in the weak and strong B-field cases at $\rho = 0.5$ are $E_r/B = 1.7$ and 0.71, respectively. This suggests that the ion flux is suppressed enough to satisfy the ambipolar condition by a weaker $E \times B$ velocity in the stronger magnetic field case, that is, in the smaller orbit width case. Therefore, apparent large discrepancy of E_r does not contradict our assertion that the FOW effect and the suppression of it by $E \times B$ drift are the important factors in determining the ambipolar electric field. In conclusion, it is found that non-local effects of loss cone particles and transit particles are important for a quantitatively reliable evaluation of ambipolar electric field.

Next, we carried out a simulation in which the electron temperature is set 1.5 times lager than in the first case. The $\Gamma_e(\rho, E_r)$-table constructed from GSRAKE is shown in Fig. 6. It has a peak around $E_r \simeq 0$, which is a typical tendency of neoclassical flux in the $1/\nu$ regime. The ambipolar condition predicted from GSRAKE is plotted in Fig. 7. Note here that the $\partial B/\partial\rho$ term is dropped in this case in order to avoid numerical ambiguity in determining the ambipolar roots from GSRAKE, as shown in Fig. 1. It is predicted that there are triple roots in the range $0.2 < \rho < 0.5$. The middle root is an unstable root, then E_r profile will be settled in either positive or negative root. The simulation result of the δf simulation is also shown in Fig. 7. One can see a good agreement of the resulting E_r profile between GSRAKE and FORTEC-3D about the radial

position where positive and negative roots appear. It takes $2.5\tau_i$ to reach the quasi-steady state plotted in this figure, which is much longer than the previous cases in which only an ion root is expected. The large negative root at the edge is formed by the orbit loss of ions. It has evolved deeper than that in Fig.1 because the simulation time is longer. It is worth noting that the edge E_r value in the simulation reached the steady state at $t \simeq 2\tau_i$ and the strong $E \times B$ rotation at the edge region prevented simulation markers from leaking out of the plasma.

The ion root E_r seen in $\rho > 0.6$ has a discrepancy between the results from GSRAKE and FORTEC-3D as it is found in Fig. 1. This can be attributed to the non-local effects and to the smallness of ambipolar $|E_r|$ of GSRAKE estimation without the $\partial B/\partial\rho$ term. On the other hand, positive root (electron root) shows a good agreement between these two numerical codes. Generally, neoclassical flux is suppressed in an electron root compared with that in an ion root. This tendency can also be seen in Fig. 9 mention later, which shows the change in Γ_i before and after the transition from the ion to electron root. The suppression of Γ_i in positive electric field means that the typical radial drift width is also suppressed in the presence of positive-E_r. Therefore, the the non-local contribution on neoclassical flux in the δf code is expected to be smaller in the electron root, and accordingly the resultant ambipolar field profiles from GSRAKE and FORTEC-3D become closer. In the middle layer $0.4 < \rho < 0.6$, the electric field profile obtained from FORTEC-3D shows an oscillatory behavior. Bifurcation of ambipolar condition occurs in this layer, and we think the oscillation is because of a numerical unstableness of FORTEC-3D at the discontinuous layer of radial electric field in the time evolution of E_r according to eq. (3). More suitable numerical method for the evolution of E_r field, which may have discontinuous points in the radial direction as shown in Fig. 7, should be adopted in the future.

The time development of E_r and Γ_i on the flux surfaces $\rho = 0.30,\ 0.35$, and 0.40 are plotted in Fig. 8 and 9, respectively. Note that the time evolution of radial electric field as well as that of weight w are stopped artificially in the initial phase until $t = 0.2\tau_i$ to avoid too much large spike at the onset of the oscillation of E_r and Γ_i. On these surfaces, the radial electric field oscillates rapidly around the negative root in the beginning phase. By taking the power spectrum, the oscillation is identified as the geodesic acoustic mode as shown in Fig. 10, of which frequency is estimated as $\omega_{GAM} = \sqrt{7}v_{th}/2R_0$[2] from neoclassical transport analysis in a simple circular-cross section tokamak case, where v_{th} is the ion thermal velocity on each flux surface. The GAM oscillation damps and E_r on each surface settles in the negative root. Then, a transition of E_r happens on $\rho = 0.30$ at $t = 0.8\tau_i$ and one can see the transition propagating to the outer surfaces in Fig. 8. Since our δf code treats the evolution of plasma as an initial value problem without any source

terms in it, the final steady E_r profile depends on the initial settings of plasma state. Therefore, there is also a possibility of steady ion root in some initial condition or by introducing source/sink terms to the simulation. Unlike in the local transport analysis like GSRAKE which solves the ambipolar condition independently on each single flux surface, evolution of ambipolar E_r profile in a global simulation is determined from the total balance of particle and momentum transport in the whole plasma region. Though the details of the triggering mechanism is still unclear because we have examined only one case, the simulation result shows that the transition and formation of ambipolar electric field has a non-local nature in it.

4 Summary

We have developed a neoclassical transport simulation code FORTEC-3D to investigate non-local and time-dependent phenomena in neoclassical transport in non-axisymmetric systems like LHD. It has been shown in this paper that the our hybrid simulation model to solve ion and electron fluxes worked successfully and that non-local neoclassical transport affects the magnitude of ambipolar electric field. It has also been found that a non-local transition mechanism is exist. Therefore, we think that the importance of using the global transport simulation model as we introduced here becomes clear in the investigation of the transport phenomena in the short time scale such as the formation and transition of ambipolar electric field in non-axisymmetric systems. We will continue to develop the δf code in order to solve the unstableness in the time evolution of E_r at the point where E_r profile changes from positive to negative root, and plan to investigate those issues above from the detailed simulation using FORTEC-3D.

As shown in Fig. 7, a strong negative E_r is formed at the edge region. It is because of the orbit loss of ions at the LCFS. The killing and recycling processes for markers adopted here are an artificial ones and do not reflect physical processes happening in the edge region of plasma such as charge exchange and re-entering of ions. Introducing such physical mechanisms will makes it possible to simulate the formation of the edge transport barrier. To introduce physical source or sink term, the procedure of marker recycling explained in Sec. 2 can be extended by adding a source term in the lhs of eq. (7). The improvement of simulation model by adding the source and sink terms will make it possible to apply the simulation to various studies concerning to neoclassical transport phenomena and to use it for the comparison with experimental data.

Acknowledgements

One of the authors (S. S.) would like to thank Prof. C. D. Beidler in Max-Planck Institute for offering us GSRAKE code. This work is performed under the auspices of the NIFS Collaborative Research Program, No. NIFS05KDAD004 and NIFS05KNXN040.

References

[1] S. V. Novakovskii *et al.*, Phys. Plasmas **4**, 4272 (1997).

[2] M. Okamoto *et al.*, J. Plasma Fusion Res. **78**, 1344 (2002).

[3] W. X. Wang *et al.*, Plasma Phys. Control. Fusion **41**, 1091 (1999).

[4] S. Brunner *et al.*, Phys. Plasmas **6**, 4504 (1999).

[5] K. C. Shaing and R. D. Hazaltine, Phys. Fluids B **4**, 2547 (1992).

[6] D. E. Hastings *et al.*, Nucl. Fusion **25**, 445 (1985).

[7] K. C. Shaing and J. D. Callen, Phys. Fluids **26**, 3315 (1983).

[8] L. M. Kovrizhnykh, Nucl. Fusion **24**, 851 (1984).

[9] S. Toda and K. Itoh, Plasma Phys. Control. Fusion **46**, 1039 (2004).

[10] C. D. Beidler *et al.*, Plasma Phys. Control. Fusion **37**, 463 (1995).

[11] C. D. Beidler and H. Maaßberg, Plasma Phys. Control. Fusion **43**, 1131 (2001).

[12] A. H. Boozer, Phys. Fluids **23**, 904 (1980).

[13] S. P. Hirshman and O. Betancourt, J. Comput. Phys. **96** 99 (1991).

[14] A. Iiyoshi *et al.*, Fusion Technol. **17**, 169 (1990).

[15] M. Wakatani, *Stellarator and Heliotron devices* (Oxford Univ. Press, New York, 1998), p. 291.

[16] S. Satake, M. Okamoto and H. Sugama, Phys. Plasmas **9**, 3946 (2002).

[17] S. Satake and M. Okamoto, J. Plasma Fusion Res. SERIES **6**, 144 (2004).

[18] S. Murakami *et al.*, Nucl. Fusion **42**, L19 (2002).

[19] H. E. Mynick, T. K. Chu, and A. H. Boozer, Phys. Rev. Lett. **48**, 322 (1982).

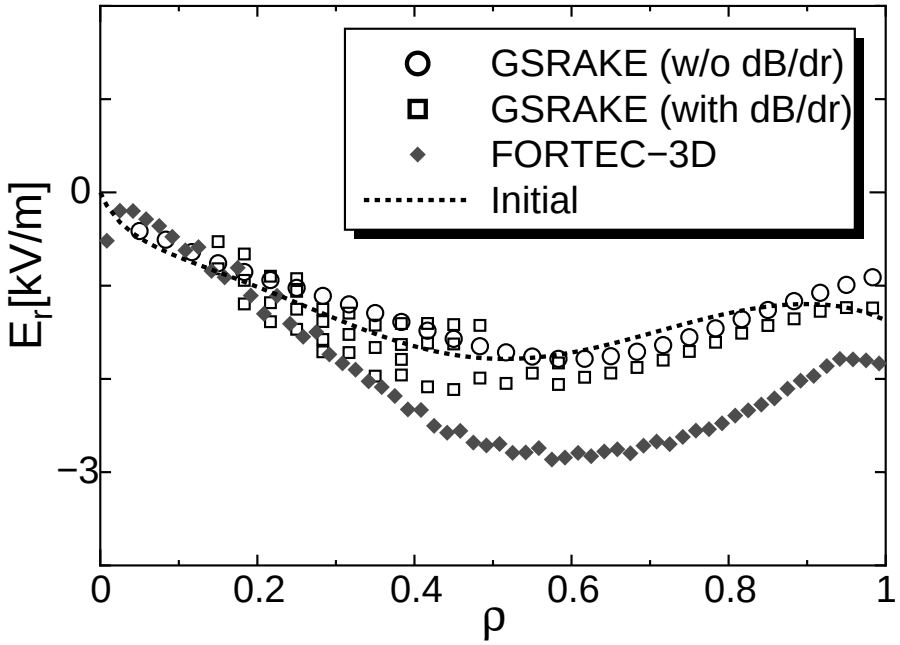

Fig. 1 : Ambipolar electric field profile in the case $B_0 = 1.65$T, $R_{ax} = 3.7$m, and $T_e = T_i = 1.0keV$ on the magnetic axis. The horizontal axis is the normalized minor radius $\rho = \sqrt{\psi/\psi_{edge}}$. Diamond marks are the simulation result of FORTEC-3D, and circles and squares are guesses from GSRAKE. The dashed line is the initial E_r profile given in FORTEC-3D.

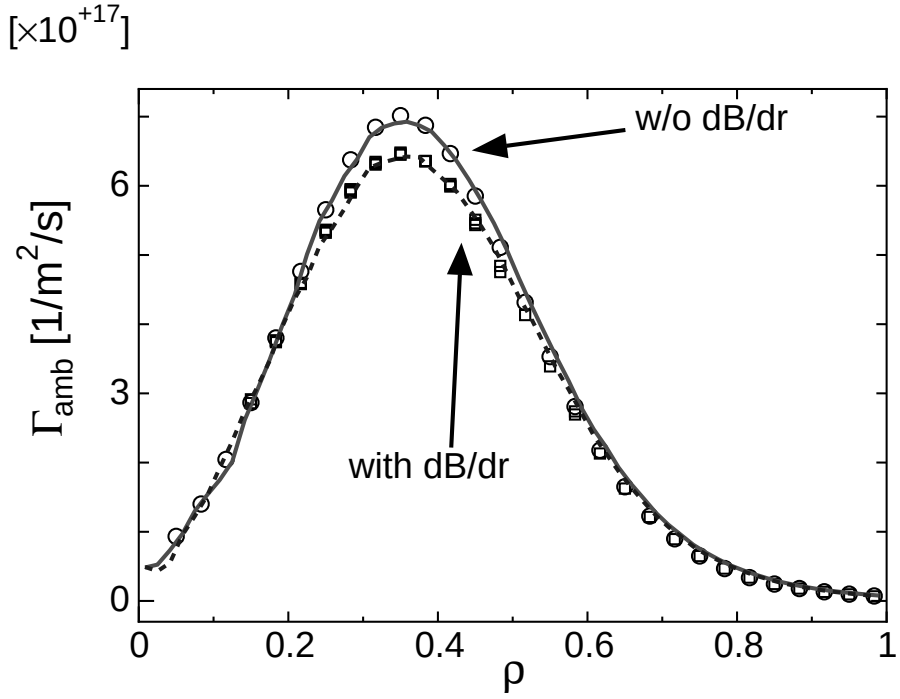

Fig. 2 : Comparison of ambipolar particle flux between GSRAKE (circles and squares) and FORTEC-3D simulations (solid and dashed lines). The circles and solid lines are results by using $\Gamma_{i,e}$-tables of GSRAKE neglecting the $\partial B/\partial\rho$ term, while this term is included in the results plotted by squares and dashed lines.

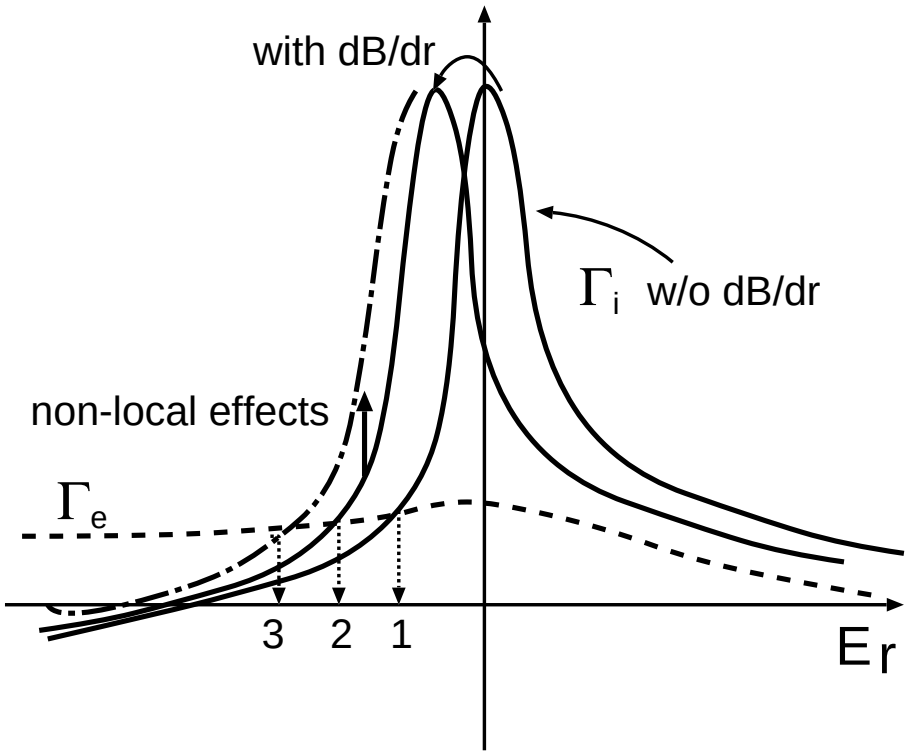

Fig. 3 : Illustration of particle fluxes Γ_i and Γ_e seen as functions of E_r. By including the $\partial B/\partial r$ term (poloidal component of ∇B drift) and non-local effects, ambipolar E_r changes $1 \rightarrow 2 \rightarrow 3$ according to the change in Γ_i.

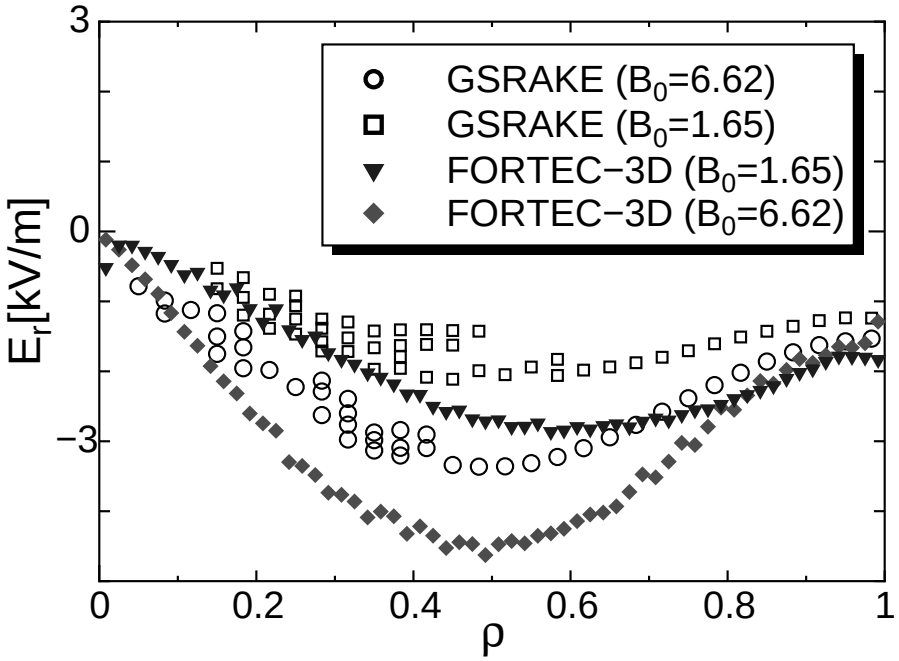

Fig. 4 : Comparison of ambipolar electric field in different strength of the magnetic field. Open circles and squares are the predictions from GSRAKE, and diamond and triangle marks are the results of FORTEC-3D at $t = 0.5\tau_i$.

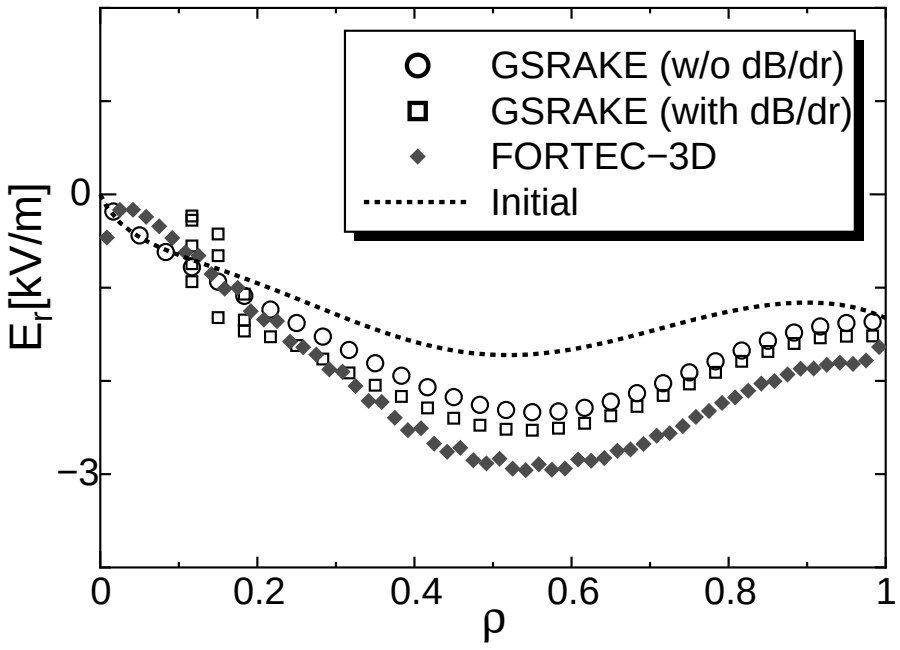

Fig. 5 : Ambipolar electric field profile in a inward-shift configuration ($R_{ax} = 3.6$m).

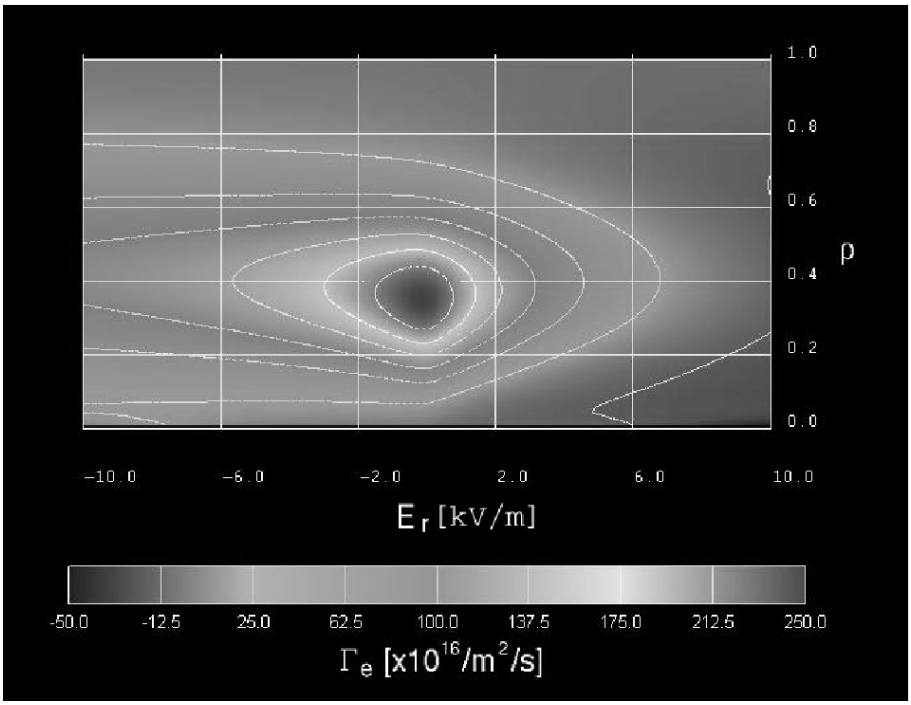

Fig. 6 : Contour-plot of Γ_e-table calculated by GSRAKE in the case $T_e = 1.5, T_i = 1.0keV$ on the magnetic axis. It has a peak at $\rho \simeq 0.35,\ E_r \simeq -1.0keV$.

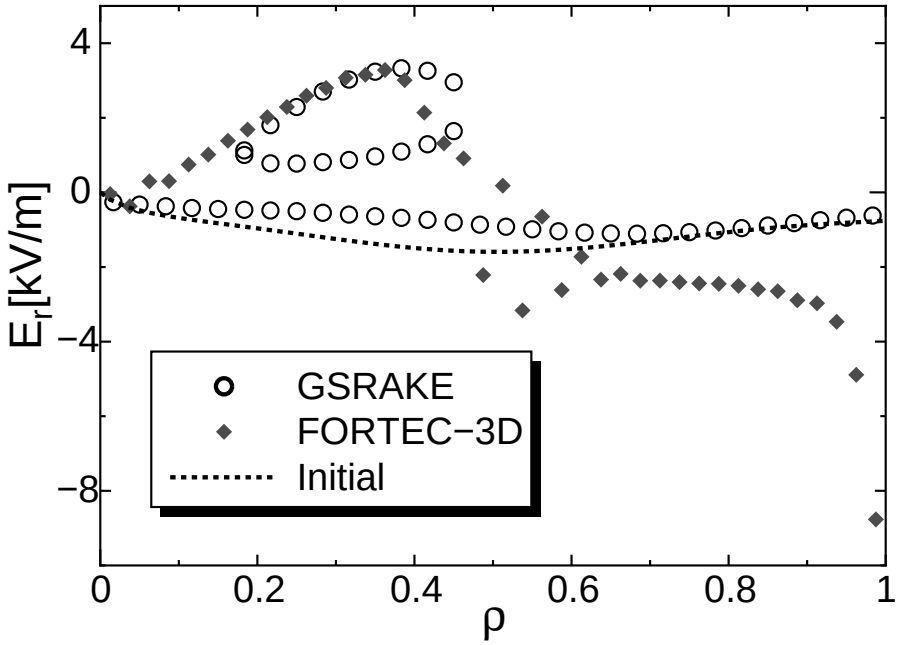

Fig. 7 : Ambipolar electric field profile simulated by using the Γ_e-table in Fig. 6 when it reaches a quasi-steady state at $t = 2.5\tau_i$. Between the region $0.2 < \rho < 0.5$, multiple roots for ambipolar condition $\Gamma_e = \Gamma_i$ is expected from GSRAKE, and the result of FORTEC-3D shows a bifurcation from negative to positive root in that region. A strong negative E_r at the edge region is formed as a result of ion orbit-loss occurred there.

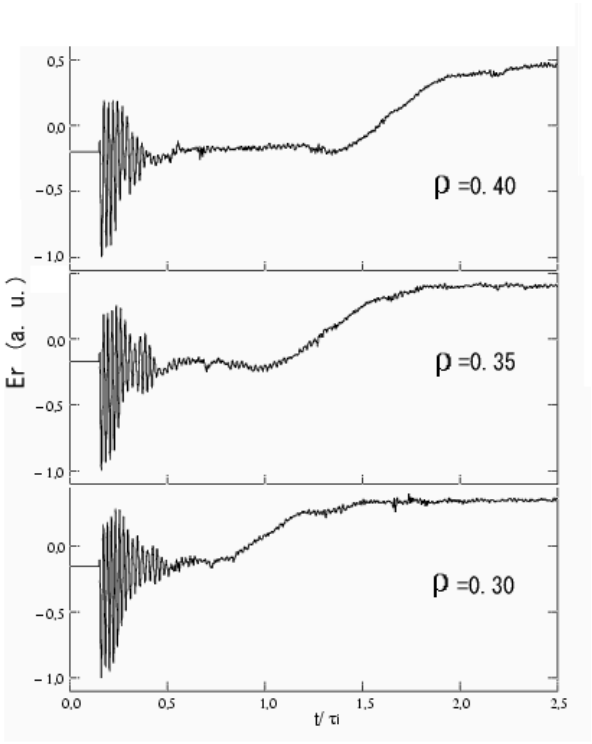

Fig. 8 : Time evolution of the radial electric field on the flux surfaces $\rho = 0.30,\ 0.35$, and 0.40 in the same case as in Fig. 7. The horizontal axis is the simulation time normalized by $\tau_i(\rho = 0.5)$.

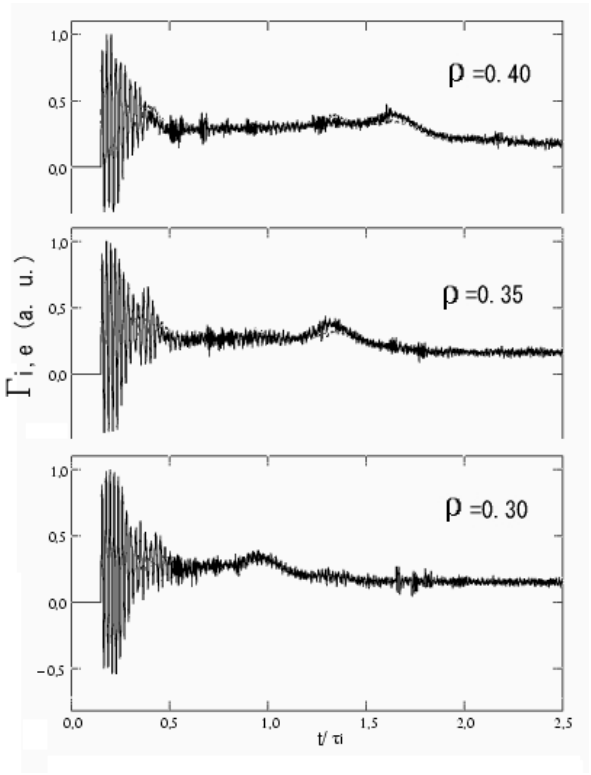

Fig. 9 : Time evolution of the radial particle fluxes on the flux surfaces $\rho = 0.30,\ 0.35$, and 0.40 in the same case as in Fig. 7. Solid line is the ion particle flux Γ_i and dashed line is Γ_e (almost hidden by the solid line).

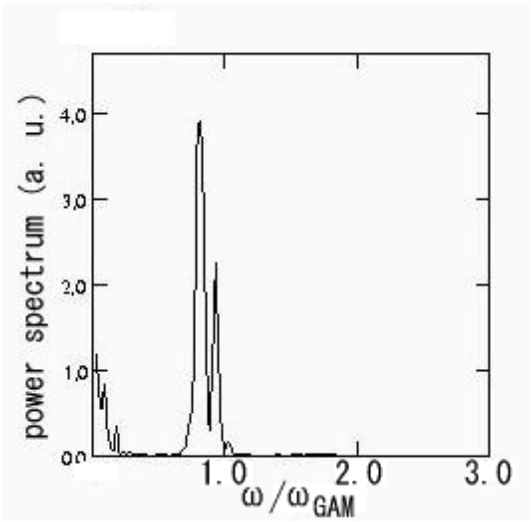

Fig. 10 : The power spectrum of E_r oscillation taken in the time span $0.2 < t/\tau_i < 0.5$ on $\rho = 0.35$ surface shown in Fig. 8. The theoretical value of GAM frequency is given by $\omega_{GAM} = \sqrt{7}v_{th}/2R_0$.